Analysis of damping ratio on the optimization of geometrically nonlinear truss structures subjected to dynamic loading

Larissa Bastos Martinelli (Main Author)
Department of Civil Engineering – Federal University of Espírito Santo
514 Fernando Ferrari Avenue, VI Technological Center, 204 Room, Vitoria, ES, 29060-970, Brazil
larissabastosm@gmail.com
https://orcid.org/0000-0002-7232-9986

Élcio Cassimiro Alves (Corresponding Author)
Department of Civil Engineering – Federal University of Espírito Santo
514 Fernando Ferrari Avenue, VI Technological Center, 204 Room, Vitoria, ES, 29060-970, Brazil
elcio.calves1@gmail.com
https://orcid.org/0000-0001-6971-2645

Manuscript Code: 13848
Date of Acceptance/Reception: 19.11.2020/17.02.2020
DOI: 10.7764/RDLC.19.3.321

Abstract
The objective of this paper is to present the formulation for optimizing truss structures with geometric nonlinearity under dynamic loads, provide pertinent case studies and investigate the influence of damping on the final result. The type of optimization studied herein aims to determine the cross-sectional areas that will minimize the weight of a given structural system, by imposing constraints on nodal displacements and axial stresses. The analyses are carried out using Sequential Quadratic Programming (SQP), available in MATLAB's Optimization Toolbox™. The nonlinear finite space truss element is defined with an updated Lagrangian formulation, and the geometrically nonlinear dynamic analysis performed herein combines the Newmark method with Newton-Raphson iterations. The dynamic analysis approach was validated by comparing the results obtained with solutions available in the literature as well as with numerical models developed with ANSYS® 18.2. A number of optimization examples of planar and space trusses under dynamic loading with geometric nonlinearity are presented. Results indicate that the consideration of damping effects may lead to a significant reduction in structural weight and that such weight reduction is proportional to increases in damping ratio.

Keywords: structural optimization, geometric nonlinearity, dynamic analysis, Damping ratio, trusses.

Introduction

The importance of considering dynamic effects and nonlinear behavior in truss structures has been well established over past decades, and current scientific literature contains numerous research focused on the development of methods to account for such phenomena. Noor & Peters (1980), for instance, presented a computational procedure for predicting the dynamic response of space trusses considering geometric and material nonlinearities. The study consisted of implementing a mixed formulation to obtain member forces, nodal velocities and nodal displacements of a given structural system. The temporal integration of the governing equations was performed by using an explicit method. Kassimali & Bidhendi (1988) studied the stability behavior and large deformation response of trusses subjected to dynamic loads. The structural analysis was performed via a combination of Eulerian formulation and the Newmark method. Zhu, Al-Bermani & Kitipornchai (1994) presented a computational procedure for predicting the geometric and material nonlinear dynamic response of space trusses, using an updated Lagrangian formulation in combination with the Newmark method. Wang et al. (2006) developed a formulation, named the vector form intrinsic finite element (VFIFE or V-5) method, for predicting the nonlinear dynamic behavior of space trusses. The study includes the solution of several numerical examples by using a combination of the newly introduced formulae and an explicit time integration method. More recently, Shi et al. (2015) derived a formulation for the analysis of fully nonlinear truss elements considering geometric and material nonlinearities. The authors presented examples of space trusses subjected to static and dynamic loads to illustrate the application of the new method.

An overview of current scientific literature focused on structural optimization shows numerous studies on trusses, frequently aimed at size optimization of these structures when subjected to static loading. However, said studies usually consider the isolated incidence of either dynamic effects or nonlinear behavior. As examples of the latter, Pyrz (1990) investigated the discrete optimization of elastic trusses with geometric nonlinearity. The study consisted of minimizing the weight of the structure by imposing constraints on element stresses, element stability and global structural stability. Saka & Ulker (1992) presented a structural optimization algorithm for geometrically nonlinear space trusses subjected to displacement, stress and cross-sectional area constraints. Results show that consideration of nonlinear behavior allows further reduction of overall weight. Suleman & Sedaghati (2005) developed a structural optimization algorithm for truss and beam structures undergoing large deflections against instability. The authors presented several benchmark

case studies and compared the results with solutions reported in the literature. Hrinda & Nguyen (2008) proposed an optimization technique for geometrically nonlinear shallow trusses with snap-through behavior subjected to stability constraints. The authors used the arc length method and a strain energy density approach within a discrete finite-element formulation.

Alternatively, current literature also provides a number of studies on size optimization of structures subjected to dynamic loading, without considering nonlinear behavior. Ohno et al. (1989) presented a computer-based methodology for minimum weight design of planar trusses subjected to multiple dynamic loads. The method imposes constraints on nodal displacement, stresses and natural frequencies. Chen (1992) proposed a weight optimization procedure using a sequential linear programming technique for the design of structures subjected to static and dynamic displacement constraints. Kocer & Arora (2002) studied the optimal design of lattice transmission towers subjected to seismic loading. Azad et al. (2018) used the big bang-big crunch algorithm to perform simultaneous size and geometry optimization of steel trusses subjected to dynamic excitations.

As previously mentioned, studies on size optimization of trusses with simultaneous incidence of dynamic and geometric nonlinear effects are seldom observed. However, researches on other types of optimization and structures involving the effects of nonlinear analysis due to dynamic loads can be found in the works by Lee & Park (2015) and Yan, Cheng & Wang (2016), where the authors carried out topological optimization studies applied to different structures. Within the same line of study, Alfouneh & Tong (2018) applied the extended unit load method to study structural nonlinearities due to dynamic loads for topological optimization problems. Cho & Choi (2000) performed a sensitivity analysis using the finite difference method for structures composed of elastic plastic materials subjected to dynamic loads and subject to large deformations and Kim et al. (2009) analyzed an airplane wing subjected to dynamic loads and the effect of non-linearities through equivalent static loads.

Moreover, procedures for optimization of structures subjected to dynamic loading usually neglect the effects of damping. As such, the understanding of how this phenomenon influences optimal design remains limited.

Given the lack of research on these subjects, this paper aims to present the formulation for optimizing truss structures with geometric nonlinearity under dynamic loads, provide case studies and investigate the influence of damping on this type of optimization process.

The Optimization Problem

The type of optimization studied herein aims to determine the cross-sectional areas that will minimize the weight of the structure, by imposing constraints on nodal displacements and axial stresses. As such, the variables of interest are the cross-sectional areas of the bars, contained in vector $\mathbf{A}$, given by Eq. (1).

$$\mathbf{A} = \{A_1, A_2, \dots A_n\} \tag{1}$$

where n represents the total number of bars of the structure. The objective function calculates the structural weight by adding up the weights of each bar, as shown in Eq. (2).

$$f(\mathbf{A}) = \sum_{i=1}^{n} \rho A_i L_i \tag{2}$$

where ρ is the density (in kg/m³), A_i is the cross-sectional area of bar i and L_i is the length of bar i. The constraints imposed on the optimization problem are given by Eqs. (3) to (6):

$$U_{max}(\mathbf{A}) \leq U_{lim} \tag{3}$$
$$\sigma_{T_{max}}(\mathbf{A}) \leq \sigma_{T_{lim}} \tag{4}$$
$$\sigma_{C_{max}}(\mathbf{A}) \leq \sigma_{C_{lim}} \tag{5}$$
$$A_{min} \leq A_i \leq A_{max} \quad i = 1, \dots, n \tag{6}$$

where $\sigma_{T_{max}}$ and $\sigma_{C_{max}}$ are the maximum values of tensile and compressive axial stresses developed in the structure, respectively; $\sigma_{T_{lim}}$ and $\sigma_{C_{lim}}$ are prescribed allowable limits for tensile and compressive stresses; U_{max} is the maximum absolute value of nodal displacement suffered by the structure; U_{lim} is the allowable nodal displacement; and A_{min} and A_{max} are the minimum and maximum limits for the design variables.

In Eqs. (3) to (5), U_{max}, $\sigma_{T_{max}}$ and $\sigma_{C_{max}}$ are nonlinear functions of the design variables, obtained with a geometrically nonlinear dynamic analysis at each iteration of the optimization process. As shown in the following Sections, the nodal displacements of the structure ($\mathbf{U}$) are obtained by solving the equation of motion of the system, which is composed by parameters that depend on the cross-sectional areas of the bars ($\mathbf{A}$), such as mass matrix ($\mathbf{M}$), damping matrix ($\mathbf{C}$) and vector of internal forces ($\mathbf{F_i}$). Likewise, the axial stresses of the bars (σ_T or σ_C) are obtained by dividing the axial force acting in each bar by its cross-sectional area. In summary, the optimization problem can be expressed by Eq. (7).

$$\begin{aligned} &\text{Find} && \mathbf{A} = \{A_1, A_2, \dots A_n\} \\ &\text{that minimizes} && f(\mathbf{A}) = \sum_{i=1}^{n} \rho A_i L_i \\ &\text{subjected to:} && \begin{cases} U_{max}(\mathbf{A}) \le U_{lim} \\ \sigma_{T_{max}}(\mathbf{A}) \le \sigma_{T_{lim}} \\ \sigma_{C_{max}}(\mathbf{A}) \le \sigma_{C_{lim}} \\ A_{min} \le A_i \le A_{max} \quad i = 1, \dots, n \end{cases} \end{aligned} \tag{7}$$

To solve this problem, a set of computational routines were executed in MATLAB® R20116a using Sequential Quadratic Programming (SQP) (Spellucci, 1998; Gould & Toint, 2004), the algorithm of which is available on MATLAB's Optimization Toolbox™. This method was chosen due to its recurrent use for solving problems with nonlinear constraints, such as the optimization problem in question.

Geometrically Nonlinear Dynamic Analysis

The governing equation of the problem is the general equation of motion of a structure, given by Eq.(8).

$$\mathbf{M\ddot{U}} + \mathbf{C\dot{U}} + \mathbf{F_i(U)} = \mathbf{F_e}(t) \tag{8}$$

in which $\mathbf{\ddot{U}}$, $\mathbf{\dot{U}}$ and $\mathbf{U}$ are the vectors of nodal accelerations, velocities and displacements, respectively; $\mathbf{M}$ is the lumped mass matrix; $\mathbf{C}$ is the damping matrix; $\mathbf{F_i}$ is the vector of internal forces, which depends on nodal displacement vector $\mathbf{U}$; and $\mathbf{F_e}$ is the time-dependent external load vector.

The transient response of the structure is obtained by solving Eq. (8), which involves the use of a time integration algorithm. The procedure shown in this paper for calculating transient response, combines the Newmark method (γ = 0.5 and β = 0.25) with Newton-Raphson iterations. A flowchart algorithm of said procedure is presented in Figure 1.

Figure 1. Geometrically nonlinear dynamic analysis procedure.

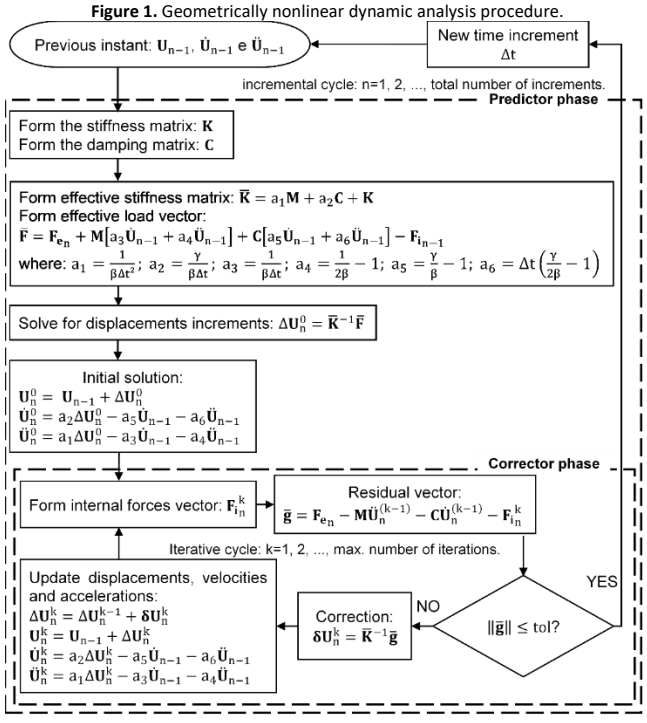

For this paper, the transient responses of interest are the nodal displacements ($\mathbf{U}$) and the axial stresses of the bars (σ). The determination of $\mathbf{U}$ is explicitly presented in Figure 1 and the axial stress of a given bar is calculated with Eq. (9).

$$\sigma_n = \frac{f_{Bx_n}}{A} \tag{9}$$

The variable f_{Bx_n} represents the internal force of node B in the x direction under configuration C_n, as presented in the following Section; A is the cross-sectional area of the bar and σ_n is the axial stress of the bar. Positive values of σ_n denote tension (σ_T), while the alternative denotes compression (σ_C).

It is important to emphasize that there are several ways to model damping, but it is usual to consider it to be viscous linear, as done in this paper, because it leads to a simpler mathematical treatment. The damping matrix ($\mathbf{C}$) is proportional to the mass ($\mathbf{M}$) and stiffness ($\mathbf{K}$) matrices, as mathematically expressed by Eq. (10).

$$\mathbf{C} = \alpha_0\mathbf{M} + \alpha_1\mathbf{K} \tag{10}$$

Here, α_0 and α_1 are the Rayleigh coefficients, calculated by adopting an appropriate damping ratio (ξ). Cook, Malkus and Plesha (1989) states that, for steel structures, the ratio varies from 0.5% to 5%. Definition of the internal force vector ($\mathbf{F_i}$) and the stiffness matrix ($\mathbf{K}$) are given in subsequent Sections.

Formulation of the Geometrically Nonlinear Element

The finite element used in this study consists of a two-node space truss element with the geometry, degrees of freedom and internal forces presented in Figure 2.

Figure 2. Space truss element: local system.

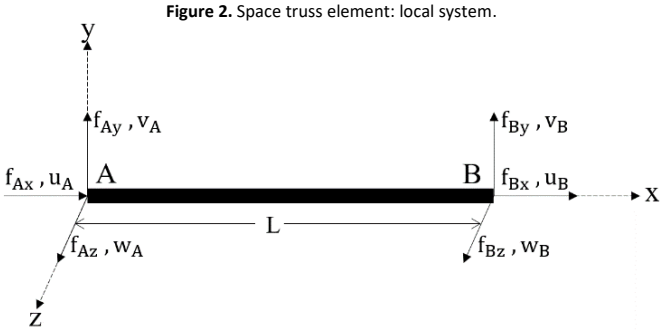

An updated Lagrangian formulation was adopted to describe the motion of this element as summarized subsequentially. For a detailed explanation of the equations depicted here, see Yang and Kuo (1994). The current deformed configuration is denoted by C_n, and the last known deformed configuration is referred to as C_{n-1}. As shown in Figure 3, element lengths under such configurations are L_n and L_{n-1}, respectively.

Figure 3. Finite element under equilibrium configurations C_n and C_{n-1}: global system.

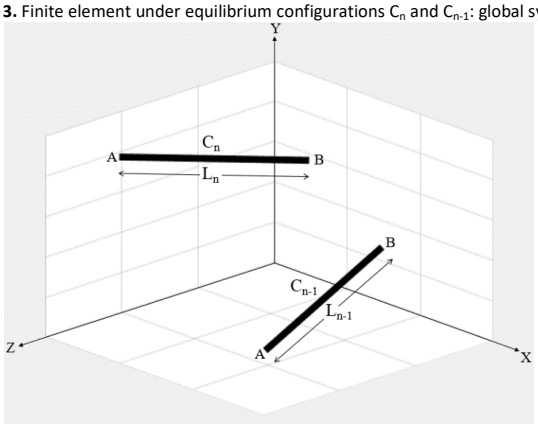

The nodal displacement generated during the incremental step from C_{n-1} to C_n is given by Eq. (11).

$$\mathbf{u} = \{u_A\ v_A\ w_A\ u_B\ v_B\ w_B\}^T \tag{11}$$

The nodal displacements in the in the x, y and z directions are represented by u, v and w, respectively. Correspondingly, the internal forces of the element under the last known deformed configuration ($\mathbf{f}_{i_{n-1}}$) and the current deformed configuration ($\mathbf{f}_{i_n}$) are shown in Eqs. (12) and (13).

$$\mathbf{f}_{i_{n-1}} = \{-f_{Bx_{n-1}}\ 0\ 0\ f_{Bx_{n-1}}\ 0\ 0\}^T \tag{12}$$

$$\mathbf{f}_{i_n} = \{-f_{Bx_n}\ 0\ 0\ f_{Bx_n}\ 0\ 0\}^T \tag{13}$$

These vectors of internal forces interact with each other, and their relation is described by Eq. (14).

$$\mathbf{f}_{i_n} = \left(\mathbf{f}_{i_{n-1}} + \Delta\mathbf{f}_i\right)\frac{L_n}{L_{n-1}} \tag{14}$$

The incremental internal force vector $\Delta\mathbf{f}_i$, is obtained from Eq. (15).

$$\Delta\mathbf{f}_i = \left\{-EA\left(\frac{L_n^2 - L_{n-1}^2}{2L_n^2}\right)\ 0\ 0\ EA\left(\frac{L_n^2 - L_{n-1}^2}{2L_n^2}\right)\ 0\ 0\right\}^T \tag{15}$$

where E is the modulus of elasticity and A is the cross-sectional area. It should be noted that the material is considered linearly elastic. The local stiffness matrix of the element ($\mathbf{k}$) is formed by five components: the elastic stiffness matrix ($\mathbf{k}_e$), the geometric stiffness matrix ($\mathbf{k}_g$) and the higher-order stiffness matrices ($\mathbf{k}_1$, $\mathbf{k}_2$ and $\mathbf{k}_3$). These matrices are defined by Eqs. (16) trough (22).

$$\mathbf{k} = \mathbf{k}_e + \mathbf{k}_g + \mathbf{k}_1 + \mathbf{k}_2 + \mathbf{k}_3 \tag{16}$$

$$\mathbf{k}_e = \frac{EA}{L_{n-1}}\begin{bmatrix} 1 & 0 & 0 & -1 & 0 & 0 \\ 0 & 0 & 0 & 0 & 0 & 0 \\ 0 & 0 & 0 & 0 & 0 & 0 \\ -1 & 0 & 0 & 1 & 0 & 0 \\ 0 & 0 & 0 & 0 & 0 & 0 \\ 0 & 0 & 0 & 0 & 0 & 0 \end{bmatrix} \tag{17}$$

$$\mathbf{k}_g = \frac{f_{Bx_{n-1}}}{L_{n-1}}\begin{bmatrix} 1 & 0 & 0 & -1 & 0 & 0 \\ 0 & 1 & 0 & 0 & -1 & 0 \\ 0 & 0 & 1 & 0 & 0 & -1 \\ -1 & 0 & 0 & 1 & 0 & 0 \\ 0 & -1 & 0 & 0 & 1 & 0 \\ 0 & 0 & -1 & 0 & 0 & 1 \end{bmatrix} \tag{18}$$

$$\mathbf{k}_1 = \frac{EA}{2L_{n-1}^2}\begin{bmatrix} \Delta u & \Delta v & \Delta w & -\Delta u & -\Delta v & -\Delta w \\ 0 & 0 & 0 & 0 & 0 & 0 \\ 0 & 0 & 0 & 0 & 0 & 0 \\ -\Delta u & -\Delta v & -\Delta w & \Delta u & \Delta v & \Delta w \\ 0 & 0 & 0 & 0 & 0 & 0 \\ 0 & 0 & 0 & 0 & 0 & 0 \end{bmatrix} \tag{19}$$

$$\mathbf{k}_2 = \frac{EA}{2L_{n-1}^2}\begin{bmatrix} 2\Delta u & 0 & 0 & -2\Delta u & 0 & 0 \\ \Delta v & \Delta u & 0 & -\Delta v & -\Delta u & 0 \\ \Delta w & 0 & \Delta u & -\Delta w & 0 & -\Delta u \\ -2\Delta u & 0 & 0 & 2\Delta u & 0 & 0 \\ -\Delta v & -\Delta u & 0 & \Delta v & \Delta u & 0 \\ -\Delta w & 0 & -\Delta u & \Delta w & 0 & \Delta u \end{bmatrix} \tag{20}$$

$$\mathbf{k}_3 = \frac{EA}{6L_{n-1}^3}\begin{bmatrix} \mathbf{h} & -\mathbf{h} \\ -\mathbf{h} & \mathbf{h} \end{bmatrix} \tag{21}$$

$$\mathbf{h} = \begin{bmatrix} 3\Delta u^2 + \Delta v^2 + \Delta w^2 & 2\Delta u\Delta v & 2\Delta u\Delta w \\ 2\Delta u\Delta v & 3\Delta v^2 + \Delta u^2 + \Delta w^2 & 2\Delta v\Delta w \\ 2\Delta u\Delta w & 2\Delta v\Delta w & 3\Delta w^2 + \Delta v^2 + \Delta u^2 \end{bmatrix} \tag{22}$$

Within each matrix, $\Delta u = u_B - u_A$, $\Delta v = v_B - v_A$ and $\Delta w = w_B - w_A$. The stiffness matrix and the vector of internal forces of the element can be represented in the global system by Eqs. (23) and (24):

$$\mathbf{k}_{\text{global}} = \mathbf{T}^T \mathbf{k} \mathbf{T} \tag{23}$$

$$\mathbf{f_i}_{\text{global}} = \mathbf{T}^T \mathbf{f_i} \tag{24}$$

where $\mathbf{T}$ is the transformation matrix. Finally, the stiffness matrix ($\mathbf{K}$) of the global system is the combination of the stiffness matrices of each element. Likewise, the vector of internal forces of the structure ($\mathbf{F_i}$) is obtained by combining the internal force vectors of each element.

Numerical Results

Six examples are presented in this Section. The first two consist of implementing the analysis procedure outlined in this paper to calculate the transient response of space trusses. To validate the geometrically nonlinear dynamic analysis, results obtained are compared with solutions available in the literature and with a finite element model generated in ANSYS® 18.2. The third example is a case study available in the literature, which is evaluated with the optimization routine. In the three following examples, the optimization routine is applied to the problem statement presented in this paper. For these last examples, the lower and upper limits chosen for the design variables are 3.04 cm² and 260 cm², respectively; the allowable values of nodal displacements were established as a fraction of the span of the structure, based on ABNT NBR 8800 (2008); and the limiting values allowed for stresses are defined by Eq. (25).

$$\sigma_{T_{\text{lim}}} = \sigma_{C_{\text{lim}}} = \frac{f_y}{\gamma_{a1}} \tag{25}$$

In Eq. (25), f_y is the yield stress, and γ_{a1} is a reduction coefficient equal to 1.1. For the sake of simplicity, the same stress limit is adopted for both tension and compression. This choice, however, neglects the onset of instability phenomena. The same mechanical properties are adopted in all three last optimization examples: $f_y = 250$ MPa, $E = 200$ GPa and $\rho = 7850$ kg/m³. To evaluate the influence of damping on the optimization process, each example considered an undamped case as well as six other damping ratios.

Example 1: Geodesic Dome – Validation of the Geometrically Nonlinear Dynamic Analysis

This example considers a geodesic dome with 24 bars and 13 nodes, shown in Figure 4a. Nodes 1 to 7 are unrestrained while nodes 8 through 13 are fixed. All bars have $E = 68992$ MPa, $\rho = 2760$ kg/m³ and $A = 6.45$ cm². The structure is subjected to the transient load shown in Figure 4b with P = 8.9 kN and T_d = 0.01 s.

Figure 4. (a) Geodesic dome (dimensions in centimeters); (b) Triangular Load.

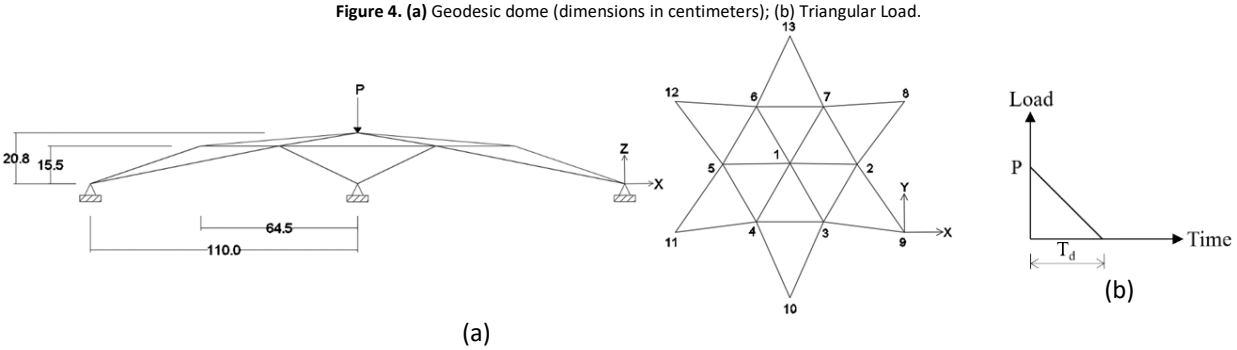

(a) (b)

This same case was previously studied by Zhu, Al-Bermani & Kitipornchai (1994) and Wang et al. (2006). As such, the same time step $\Delta t = 1.56 \times 10^{-4}$ s and damping ratio ξ = 0% are reproduced in this analysis. Figure 5 shows good agreement between the transient response of node 1 obtained in this paper, and the one presented in the aforementioned literature.

Example 2: Lattice Beam – Validation of the Geometrically Nonlinear Dynamic Analysis

Figure 6a shows a lattice beam with 76 bars and 28 nodes, and Figure 6b shows the load used in this analysis (P = 50 kN). Mechanical properties were fixed for all bars, with $E = 71700$ MPa, and $\rho = 4152$ kg/m³. However, three groups

with distinct cross-sectional areas are considered. For group 1, $A = 0.8\ cm^2$, group 2 has $A = 0.6\ cm^2$ and group 3, $A = 0.4\ cm^2$. Nodes 1, 7, 8, 14, 15, 21, 22 and 28 are fixed.

Figure 5. Geodesic dome: displacement of node 1 in the z direction.

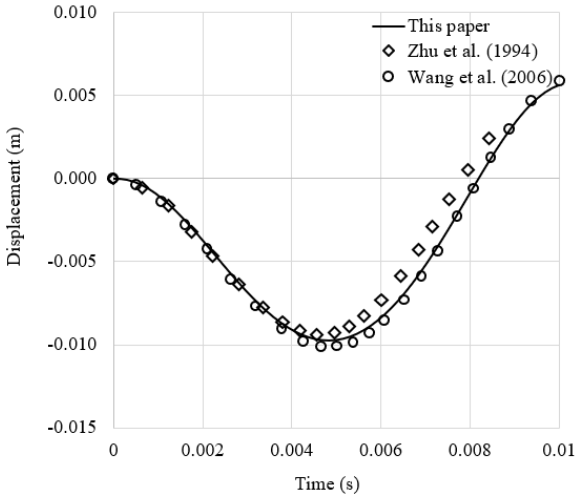

Figure 6. Lattice beam: a) dimensions in meters; b) step load.

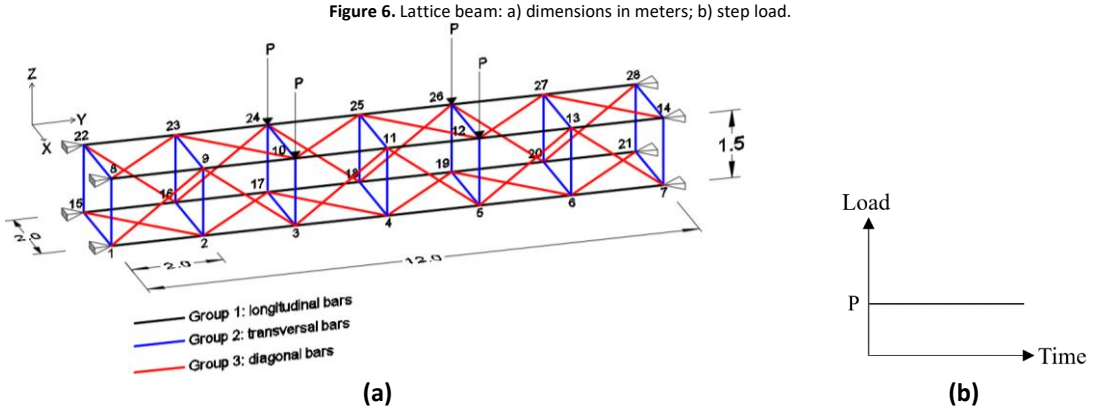

A time step of $\Delta t = 10^{-5}$ s was used in the geometrically nonlinear dynamic analysis. Figure 7, compares the transient response of node 10 with the one obtained with ANSYS® 18.2. Acceptable agreement is observed for ξ = 0% and ξ = 5%.

Figure 7. Lattice beam: displacement of node 10 in the z direction.

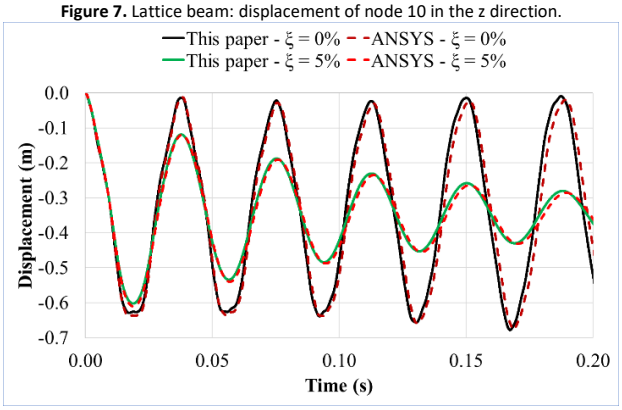

Example 3: Planar truss with ten bars – Compared optimization

This example consists of a planar truss with 10 bars and 6 nodes. Figure 8a shows its geometry, loading and boundary conditions. All bars have $\rho = 7860\ kg/m^3$, $A = 3.14\ cm^2$ and $f_y = 200$ MPa. The structure is subjected to the dynamic load presented in Figure 8b.

Figure 8. Planar truss: a) geometry, loading and boundary conditions; b) dynamic load. Source: Kim & Park (2010).

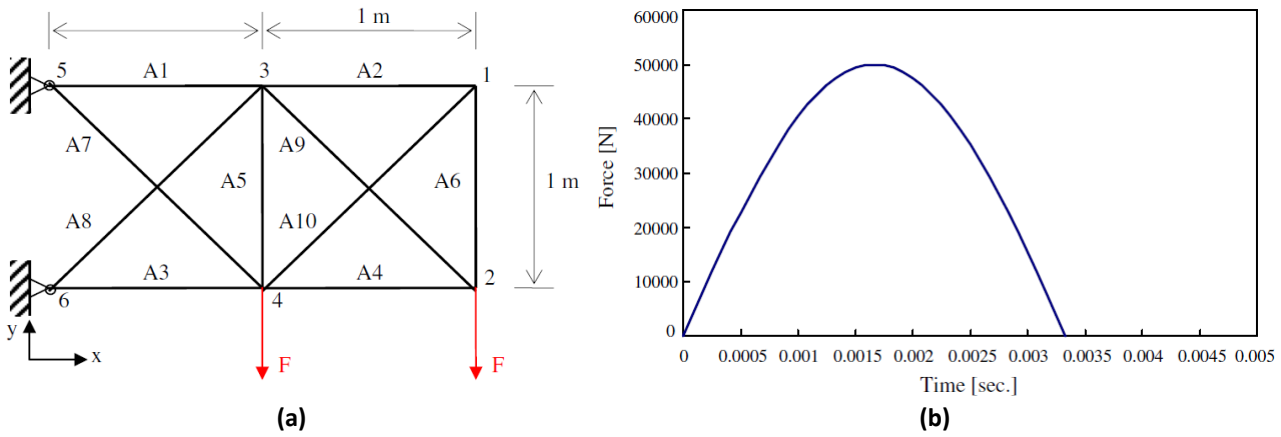

This same case was previously studied by Kim & Park (2010). In the original example, the authors studied the material nonlinearity of the structure, considering a bilinear elastoplastic strain-stress curve, with Young's modulus of 200 GPa and tangent modulus of 50 GPa. In this paper, the structure is considered geometrically nonlinear and the material is linear elastic, with $\mathrm{E} = 50$ GPa.

The same parameters used by Kim & Park (2010) are reproduced in this paper: limiting value for tensile and compressive stresses is 250 MPa; lower and upper limits for the design variables are 0.785 cm² and 28.26 cm², respectively; duration time of the dynamic load is 0.0033 s; total analysis time is 0.03 s; time step is 0.0002 s; and damping ratio ξ = 0%. The initial design and the optimization results obtained are shown in Table 1.

Table 1. Initial design and optimization results for the planar truss.

	Initial design	Optimization results	
		Kim and Park (2010)	This paper
A1 (cm²)	3.14	4.976	4.1327
A2 (cm²)	3.14	0.955	1.9422
A3 (cm²)	3.14	4.806	5.1792
A4 (cm²)	3.14	1.569	1.0745
A5 (cm²)	3.14	0.786	4.6656
A6 (cm²)	3.14	0.786	2.8912
A7 (cm²)	3.14	3.163	3.6533
A8 (cm²)	3.14	3.368	2.0882
A9 (cm²)	3.14	2.099	1.1152
A10 (cm²)	3.14	1.138	1.8695
Weight (kg)	28.77	21.77	25.33
σ_{max} (MPa)	323.7	249	250

As previously mentioned, Kim & Park (2010) studied a different type of nonlinearity than the one adopted in this paper. Therefore, it was expected that the results obtained were not the same. However, comparing both results allows to observe the influence of each nonlinearity in this case study. Kim & Park (2010) considered material nonlinearity and achieved a weight reduction of 24.33%, while the procedure used in this paper for geometrical nonlinearity resulted in a structure only 11.96% lighter than the initial design. Thus, studying this example considering material nonlinearity leads to almost double weight reduction than considering geometrical nonlinearity.

Example 4: Geodesic Dome – Optimization

In this case the optimization procedure is applied to the geodesic dome of Example 1. The geometry and load profile presented in Figure 4 are reproduced here. However, for this case $\mathrm{f_y} = 250$ MPa, $\mathrm{E} = 200$ GPa, $\rho = 7850$ kg/m^3, P = 356 kN and Td = 0.1 s. Three groups of bars are considered, as shown in Figure 9.

Figure 9. Geodesic dome: group of bars.

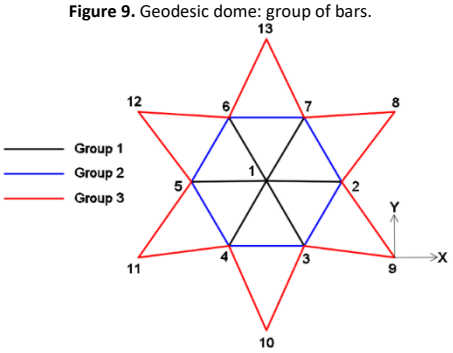

The limiting value of nodal displacement was fixed at 0.007 m, while the limit for tensile and compressive stresses was set at 227 MPa. For the dynamic analysis performed in the optimization process, a duration of 0.1 s and a time step Δt = 0.0001 s were adopted. The initial design and the optimization results obtained for different values of damping ratio are shown in Table 2.

Table 2. Initial design and optimization results for the geodesic dome.

	Initial design	Optimization results						
		ξ = 0%	ξ = 0.5%	ξ = 1%	ξ = 2%	ξ = 3%	ξ = 4%	ξ = 5%
A1 (cm²)	260	193.5808	189.8994	188.4265	185.6098	182.9248	180.3367	177.8271
A2 (cm²)	260	177.4242	191.6735	189.6515	185.7113	181.9262	178.3112	174.8597
A3 (cm²)	260	22.3056	16.2275	16.5639	17.1837	17.7396	18.2374	18.6856
Weight (kg)	3532.8577	1296.6764	1283.1640	1275.0522	1259.1391	1243.6198	1228.4773	1213.6991
U_{max} (m)	-	0.007	0.007	0.007	0.007	0.007	0.007	0.007
$\sigma_{T_{max}}$ (MPa)	-	91.2696	101.7165	78.2718	56.5276	56.7036	56.9169	57.1421
$\sigma_{C_{max}}$ (MPa)	-	161.0229	213.7410	207.8548	197.2475	187.9259	179.676	172.3087
Number of iterations	-	46	31	39	32	37	31	24
Number of objective function evaluations	-	458	216	303	238	326	341	191

The comparative graph in Figure 10, indicates that variation of damping does not result in a significant reduction in weight. With ξ = 0.5%, the structure is only 1% lighter than the undamped case, likely due to the high rigidity of the structure. When the damping ratio is increased to 1%, the structure becomes 0.6% lighter in comparison with ξ = 0.5%. Additional increments of damping ratio, up to 5%, all indicate a weight reduction of 1.2% in relation to each previous increment.

Figure 10. Geodesic dome: weight percentage reduction obtained for various damping ratios.

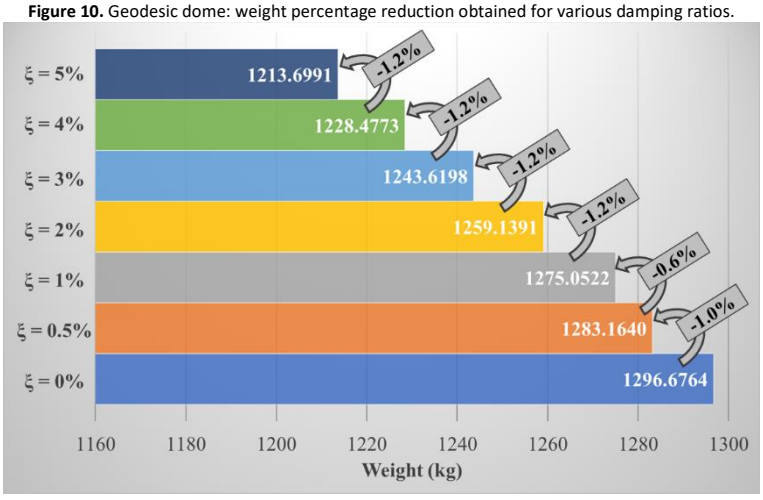

Example 5: Lattice Beam – Optimization

Analogously to the previous example, the second optimization study reproduces the geometry, general load profile and groups of bars from Example 2. For this example, however, $f_y = 250$ MPa, $E = 200$ GPa, $\rho = 7850$ kg/m^3 and P = 100 kN. The limit value of nodal displacement was set at 0.034 m and stresses are constrained to 227 MPa. A duration of 0.5 s and a time step Δt = 0.001 s are adopted for the dynamic analysis. The initial design and the optimization results obtained for different values of damping ratio are shown in Table 3.

Table 3. Initial design and optimization results for the latticed beam.

	Initial design	Optimization results						
		ξ = 0%	ξ = 0.5%	ξ = 1%	ξ = 2%	ξ = 3%	ξ = 4%	ξ = 5%
A1 (cm²)	260	22.4222	15.3036	15.1937	15.0009	14.8071	14.6117	14.4168
A2 (cm²)	260	7.7398	7.2404	7.0456	6.6952	6.3997	6.1557	5.9663
A3 (cm²)	260	19.3697	16.0712	15.8582	15.4489	15.068	14.7177	14.3972
Weight (kg)	32848.0837	2114.8170	1661.8152	1639.4898	1598.1998	1560.4130	1526.0832	1495.3670
U_{max} (m)	-	0.015043	0.019020	0.019008	0.018993	0.018999	0.019016	0.019035
$\sigma_{T_{max}}$ (MPa)	-	189.1810	227	227	227	227	227	227
$\sigma_{C_{max}}$ (MPa)	-	227	227	227	227	227	227	227
Number of iterations	-	43	30	33	35	38	33	33
Number of objective function evaluations	-	406	225	221	413	329	293	249

As opposed to neglecting damping effects, Figure 11 shows that the use of a rather small damping ratio such as 0.5%, is enough to generate a significant reduction of weight, of 21%. From this point on, however, variations in damping bear no significant effect on structural weight if compared with each previous increment, with all subsequent weight reductions falling within the range of 1-2%.

Figure 11. Lattice beam: weight percentage reduction obtained for various damping ratios.

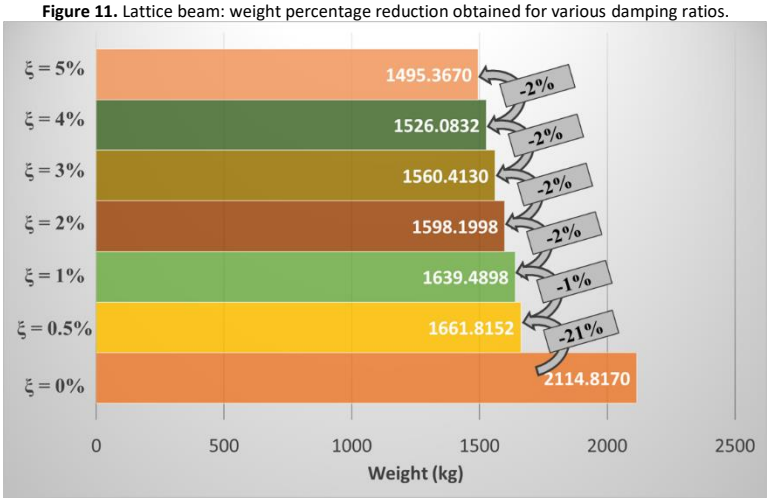

Example 6: Transmission Tower – Optimization

This example consists of a transmission tower with 47 bars and 22 nodes (Figure 12a). All nodes are free to move with the exception of nodes 21 and 22 which are fixed. The structure is subjected to the general load profile shown in Figure 12b, representing the weight of the cables and the wind load acting on the tower. Bar grouping and load values applied to each node are shown in Figure 12b.

Limiting values allowed for nodal displacement and all stresses are set at 0.08 m and 227 MPa, respectively. A duration of 1 s and a time step Δt = 0.01 s are adopted for the dynamic analysis performed throughout the optimization procedure.

Figure 12. Transmission tower (a) dimensions given in meters; (b) applied loading and groups of bars (loads given in Newtons).

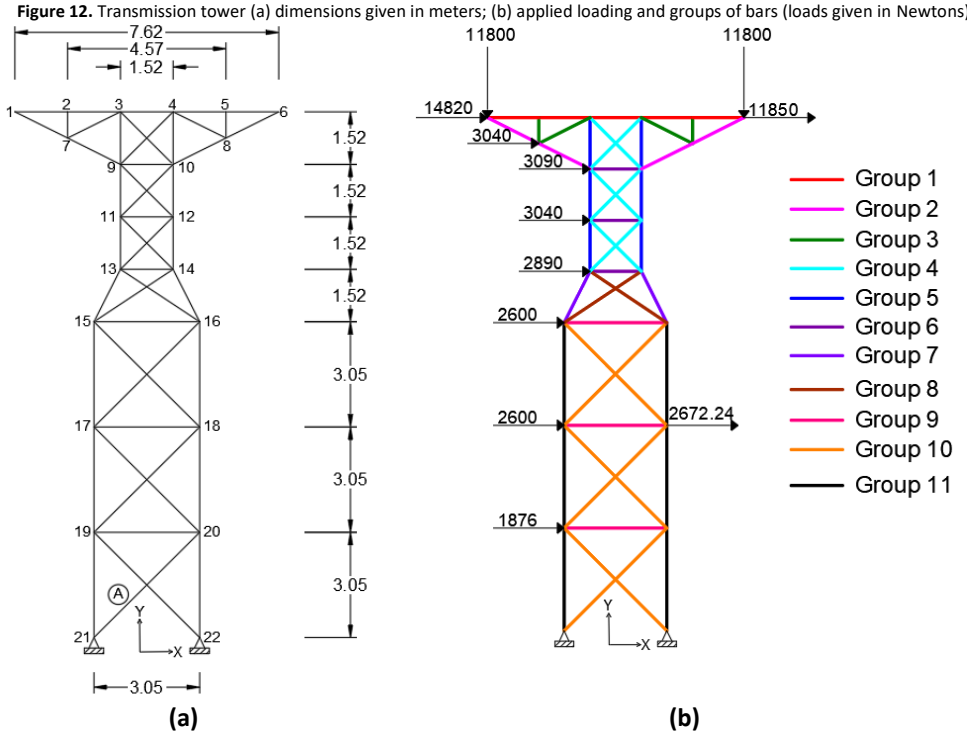

Table 4 presents the initial design used and the optimization results obtained for different values of damping ratio. The transient response of node 6 after optimization, for all damping ratios, is shown in Figue 13. Figure 14 shows the axial stress of bar A over time.

Table 4. Initial design and optimization results for the transmission tower.

	Initial design	Optimization results						
		ξ = 0%	ξ = 0.5%	ξ = 1%	ξ = 2%	ξ = 3%	ξ = 4%	ξ = 5%
A1 (cm²)	260	10.8159	3.0400	3.0400	3.0400	3.0400	3.0400	3.0400
A2 (cm²)	260	3.0400	3.0400	3.0400	3.0400	3.0400	3.0400	3.0400
A3 (cm²)	260	3.0400	3.0400	3.0400	3.0400	3.0400	3.0400	3.0400
A4 (cm²)	260	4.8099	3.0400	3.0400	3.0400	3.0400	3.0400	3.0400
A5 (cm²)	260	10.9227	6.3976	6.3057	6.1223	6.0835	6.1106	6.1368
A6 (cm²)	260	3.0400	3.0400	3.0400	3.0400	3.0400	3.0400	3.0400
A7 (cm²)	260	15.6703	13.6533	13.4943	13.1851	13.0487	12.9892	12.9282
A8 (cm²)	260	4.6436	3.8368	3.7894	3.6949	3.6632	3.6581	3.6524
A9 (cm²)	260	3.0400	3.0400	3.0400	3.0400	3.0400	3.0400	3.0400
A10 (cm²)	260	3.6654	4.1631	4.1654	4.1714	4.1336	4.0754	4.0180
A11 (cm²)	260	19.2338	20.2782	20.1900	20.0230	19.8096	19.5732	19.3391
Weight (kg)	22076.0900	664.9780	584.3981	581.8902	577.0689	572.4562	567.8903	563.3601
U_{max} (m)	-	0.08	0.08	0.08	0.08	0.08	0.08	0.08
$\sigma_{T_{max}}$ (MPa)	-	193.5679	183.6943	182.0174	178.6671	177.5891	177.5664	177.5423
$\sigma_{C_{max}}$ (MPa)	-	201.6504	214.3881	205.1776	208.0514	208.3433	206.3747	204.4334
Number of iterations	-	152	60	55	78	43	50	39
Number of objective function evaluations	-	2100	891	822	1248	605	707	550

Figure 13. Transmission tower: displacement of node 6 in x direction.

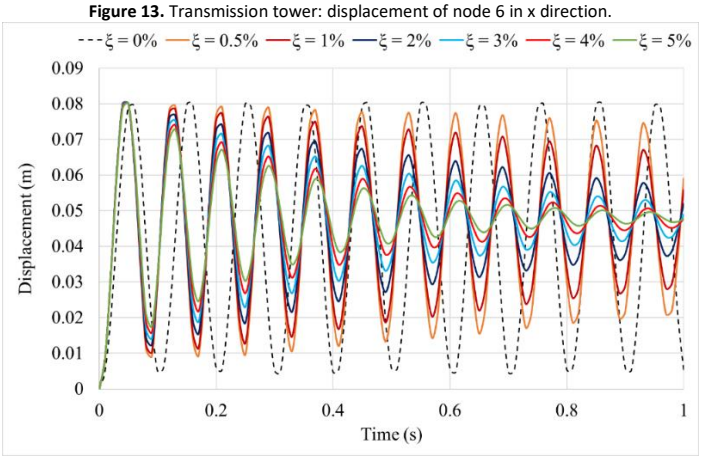

Figure 14. Transmission tower: axial stress of bar A.

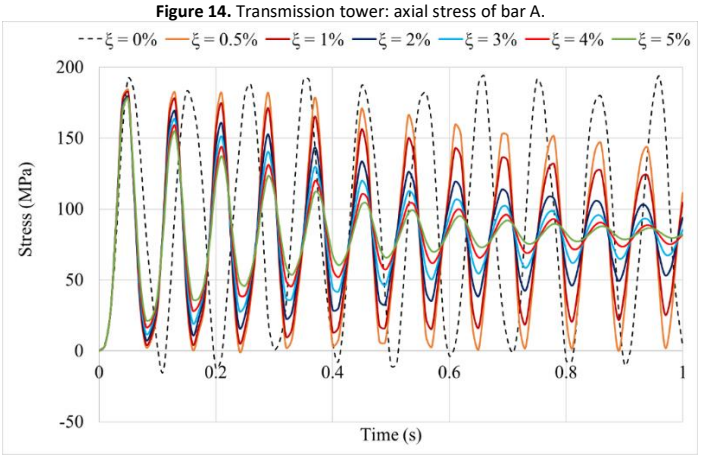

In a manner similar to Example 5, Figure 15 indicates that the consideration of a 0.5% damping ratio results in significant weight reduction, 12.1% in this case. Furthermore, in accordance with results obtained in all previous optimization examples, it seems that further increments in damping ratio cease to significantly affect structural weight.

Figure 15. Transmission tower: weight percentage reduction obtained for various damping ratios.

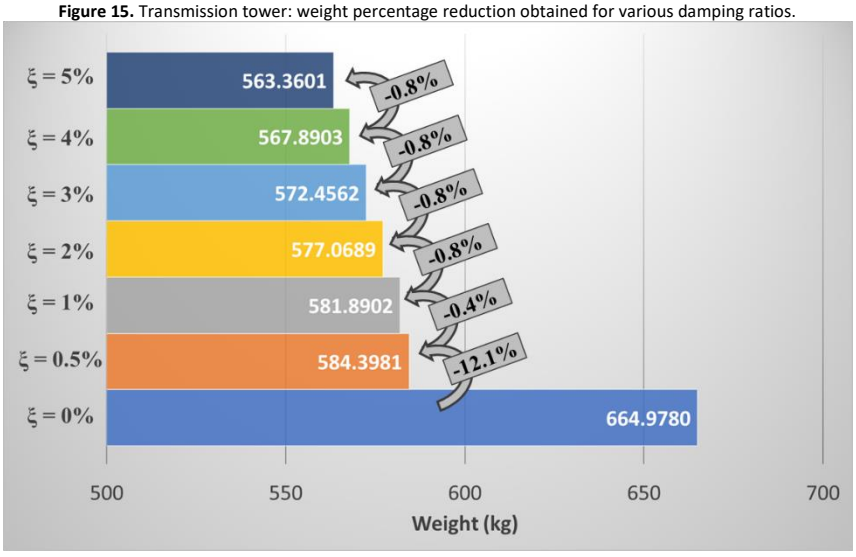

Conclusions

In this paper, a set of computational routines were performed in MATLAB to study the optimization of geometrically nonlinear truss structures subjected to dynamic loading, using the SQP algorithm available on MATLAB's Optimization Toolbox™. The formulated optimization problem sought to determine the cross-sectional areas that would minimize the weight of the structure, imposing constraints on nodal displacements and axial stresses.

As these constraints imply the necessity to perform a geometrically nonlinear dynamic analysis at each iteration of the optimization process, the first two examples were dedicated to validating the analysis procedure. The transient response of the space trusses was calculated, and the results obtained were consistent with solutions available in the literature and with results generated by ANSYS® 18.2. Therefore, the analysis procedure is considered validated.

In Example 3, an optimization case study available in the literature was evaluated, comparing the influence of different nonlinear behaviors. Results showed that considering material nonlinearity may lead to almost double weight reduction than considering geometrical nonlinearity.

In Examples 4 to 6, the optimization process was used in order to study space and planar trusses. Results showed a significant reduction of weight if damping is accounted for in the second and third examples. As opposed to neglecting damping effects, the consideration of a damping ratio of $\xi = 0.5\%$ resulted in 21% weight reduction of the lattice beam and 12.1% of the transmission tower. However, in the first example this reduction of weight was not as substantial. The geodesic dome exhibits a structural weight reduction of just 1% with $\xi = 0.5\%$ when compared with $\xi = 0\%$. This is likely due to the higher rigidity of the geodesic dome in comparison with the other two structures.

Furthermore, it was observed that in all three last optimization examples, the increase of damping ratio was proportional to the reduction of weight. A 0.5% increment in ξ on the geodesic dome (from $\xi = 0.5\%$ to $\xi = 1\%$) caused a reduction of weight of 0.6%. Subsequentially, doubling the increase in damping ratio also caused the reduction in weight to double to 1.2%. The remaining optimization studies also show analogous responses starting at the second damping ratio increment of $\xi = 0.5\%$ to $\xi = 1\%$. Further increases of 1% in ξ doubled the weight reduction of the lattice beam from 1% to 2%, while the transmission tower shows a difference from 0.4% to 0.8% in weight within the same range of damping ratio values.

Acknowledgements

The authors would like to acknowledge the financial support provided by CAPES (Coordination for the Improvement of Higher Education Personnel).

References

ABNT NBR 8800: Design of Steel and Composite Structures for Buildings. Rio de Janeiro (2008)

Alfouneh, M., Tong, L. (2018). Topology optimization of nonlinear structures with damping under arbitrary dynamic loading. *Struct. Multidisc. Optim.*, 57, 759–774. doi: 10.1007/s00158-017-1765-6

Azad, S. K., Bybordiani, M., Azad, S. K., Jawad, F. K. J. (2018). Simultaneous size and geometry optimization of steel trusses under dynamic excitations. *Struct. Multidiscip. Optim.,* 58, 2545-2563.

Chen, T. -Y. (1992). Design optimization with static and dynamic displacement constraints. *Struct. Optim.*, 4(3-4), 179–185.

Cho, S., Choi, K. K. (2000). Design sensitivity analysis and optimization of nonlinear transient dynamics. Part I-sizing design. *Int. J. Numer. Methods Engrg*., 48, 351–373.

Cook, R. D., Malkus, D. S., Plesha, M. E. (1989). *Concepts and applications of finite element analysis.* John Wiley & Sons.

Gould, N., Toint, P. L. (2004). Preprocessing for quadratic programming. *Math. Programming.,* 100, 95–132.

Hrinda, G. A., Nguyen, D. T. (2008). Optimization of stability-constrained geometrically nonlinear shallow trusses using an arc length sparse method with a strain energy density approach. *Finite Elem. Anal. Des.,* 44(15), 933-950.

Kassimali, A., Bidhendi, E. (1988). Stability of trusses under dynamic loads. *Comput. Struct.*, 29(3), 381-392.

Kim, Y. I., Park, G. J., Kolonay, R. M., Blair, M., Canfield, R. A. (2009). Nonlinear dynamic response structural optimization of a joined-wing using equivalent static loads. *J. Aircraft*, 46(3), 821–831.

Kim, Y. -I., Park, G. -J. (2010). Nonlinear dynamic response structural optimization using equivalent static loads. *Comput. Methods Appl. Mech. Engrg.*, 199, 660-676.

Kocer, F. Y., Arora, J. S. (2002). Optimal Design of Latticed Towers Subjected to Earthquake Loading. *J. Struct. Eng.*, 128(2), 197-204.

Lee, H. A, Park, G. J. (2015). Nonlinear dynamic response topology optimization using the equivalent static loads method. *Comput. Methods Appl. Mech. Engrg.,* 283, 956-970.

Noor, A. K., Peters, J. M. (1980). Nonlinear dynamic analysis of space trusses. *Comput. Methods Appl. Mech. Eng.*, 21(2), 131-151.

Ohno, T., Kramer, G. J. E., Grierson, D. E. (1989). Least-weight design of frameworks under multiple dynamic loads. *Struct. Optim.,* 1(3), 181–191.

Pyrz, M. (1990). Discrete optimization of geometrically nonlinear truss structures under stability constraints. *Struct. Optim.*, 2(2), 125–131.

Saka, M. P., Ulker, M. (1992). Optimum design of geometrically nonlinear space trusses. *Comput. Struct.*, 42(3), 289-299.

Shi, H., Salim, H., Shi, Y., Wei, F. (2015). Geometric and material nonlinear static and dynamic analysis of space truss structures. *Mech. Based Des. Struct. Mach.*, 43, 38-56.

Spellucci, P. (1998). A new technique for inconsistent QP problems in the SQP method. *Mathematical Methods of Operations Research*, 47(3), 355-400.

Suleman, A., Sedaghati, R. (2005). Benchmark case studies in optimization of geometrically nonlinear structures. *Struct. Multidiscip. Optim.*, 30(4), 273-296.

Wang, C. -Y., Wang, R. -Z., Chuang, C. -C., Wu, T. -Y. (2006). Nonlinear dynamic analysis of reticulated space truss structures. *J. Mech.,* 22(3), 199-212.

Yan, K., Cheng, G., Wang, B. P. (2016). Topology optimization of plate structures subject to initial excitations for minimum dynamic performance index. *Struct. Multidiscip. Optim.,* 53, 623-633.

Yang, Y. -B., Kuo, S. -R. (1994). *Theory and analysis of nonlinear framed structures*. Prentice Hall, New York.

Zhu, K., Al-Bermani, F. G. A., Kitipornchai, S. (1994). Nonlinear dynamic analysis of lattice structures. *Comput. Struct.*, 52(1), 9-15.